Laboratory experiments on counter-propagating collisions of solitary waves. Part 1. Wave interactions

Citation	Chen, Y., & Yeh, H. (2014). Laboratory experiments on counter-propagating collisions of solitary waves. Part 1. Wave interactions. Journal of Fluid Mechanics, 749, 577-596. doi:10.1017/jfm.2014.231
DOI	10.1017/jfm.2014.231
Publisher	Cambridge University Press
Version	Version of Record
Terms of Use	http://cdss.library.oregonstate.edu/sa-termsofuse

J. Fluid Mech. (2014), *vol.* 749, *pp.* 577–596.
doi:10.1017/jfm.2014.231

Laboratory experiments on counter-propagating collisions of solitary waves. Part 1. Wave interactions

Yongshuai Chen and Harry Yeh†

School of Civil and Construction Engineering, Oregon State University, Corvallis, OR 97331-3212, USA

(Received 16 November 2013; revised 17 April 2014; accepted 17 April 2014;
first published online 19 May 2014)

Collisions of counter-propagating solitary waves are investigated experimentally. Precision measurements of water-surface profiles are made with the use of the laser induced fluorescence (LIF) technique. During the collision, the maximum wave amplitude exceeds that calculated by the superposition of the incident solitary waves, and agrees well with both the asymptotic prediction of Su & Mirie (*J. Fluid Mech.*, vol. 98, 1980, pp. 509–525) and the numerical simulation of Craig *et al.* (*Phys. Fluids*, vol. 18, 2006, 057106). The collision causes attenuation in wave amplitude: the larger the wave, the greater the relative reduction in amplitude. The collision also leaves imprints on the interacting waves with phase shifts and small dispersive trailing waves. Maxworthy's (*J. Fluid Mech.*, vol. 76, 1976, pp. 177–185) experimental results show that the phase shift is independent of incident wave amplitude. On the contrary, our laboratory results exhibit the dependence of wave amplitude that is in support of Su & Mirie's theory. Though the dispersive trailing waves are very small and transient, the measured amplitude and wavelength are in good agreement with Su & Mirie's theory. Furthermore, we investigate the symmetric head-on collision of the highest waves possible in our laboratory. Our laboratory results show that the runup and rundown of the collision are not simple reversible processes. The rundown motion causes penetration of the water surface below the still-water level. This penetration causes the post-collision waveform to be asymmetric, with each departing wave tilting slightly backward with respect to the direction of its propagation; the penetration is also the origin of the secondary dispersive trailing wavetrain. The present work extends the studies of head-on collisions to oblique collisions. The theory of Su & Mirie, which was developed only for head-on collisions, predicts well in oblique collision cases, which suggests that the obliqueness of the collision may not be important for this 'weak' interaction process.

Key words: shallow water flows, solitary waves, waves/free-surface flows

1. Introduction

Solitary waves can be described by an exact solution to the Korteweg–de Vries (KdV) equation which models water waves propagating in a single direction $+x$ in

† Email address for correspondence: harry@engr.orst.edu

finite-but-shallow water. The KdV equation can be written as:

$$\eta_t + c_0\eta_x + \frac{3}{2}\frac{c_0}{h_0}\eta\eta_x + \frac{1}{6}c_0h_0^2\eta_{xxx} = 0, \tag{1.1}$$

where η is the water-surface elevation from the equilibrium state, h_0 is the quiescent water depth, which is constant, and $c_0 = \sqrt{gh_0}$ in which g is the gravitational acceleration, and t is time. The solitary wave is expressed as:

$$\eta = a\,\mathrm{sech}^2\left\{\sqrt{\frac{3a}{4h_0^3}}\left(x - c_0\left(1 + \frac{a}{2h_0}\right)t\right)\right\}, \tag{1.2}$$

where a is the wave height. These solitary waves possess the characteristics of a soliton (Zabusky & Kruskal 1965), which is 'a localized nonlinear wave which interacts with another (arbitrary) local disturbance and regains asymptotically its exact initial shape and velocity (allowing for a possible phase shift)' (Ablowitz & Segur 1981). Therefore, solitary waves are often called KdV solitons. Zabusky & Kruskal (1965) predicted that when a larger soliton catches up to and collides with a smaller one from behind, a 'strong' nonlinear overtaking interaction takes place and the collision process is considered as 'elastic'. After the collision, each solitary wave re-emerges retaining its original identity with the only remnant of the interaction being a shift in phase: the faster wave is shifted forward and the slower wave is shifted backward. This phenomenon was demonstrated experimentally by Weidman & Maxworthy (1978), and more quantitatively by Craig *et al.* (2006) and Li (2012).

On the other hand, the interaction is 'weak' when two solitary waves moving in opposite directions collide head-on with each other. The weak interaction of two solitary waves is the theme of this paper. Maxworthy (1976) first demonstrated experimentally the head-on collision process. The present paper revisits Maxworthy's laboratory investigation with the use of a more precise apparatus and more accurate instruments to make unambiguous and quantitative comparisons with the theory and the numerical results for this nonlinear collision process.

In the companion paper Chen, Zhang & Yeh (2014, Part 2), the induced flow field during the collisions of counter-propagating solitary waves is investigated experimentally with the use of the particle image velocimetry (PIV). In particular, the flows near the bed are visualized and analyzed in terms of velocities, accelerations, vorticities, and velocity-gradient tensors.

2. Background

Byatt-Smith (1971) first showed that the maximum amplitude of head-on collision of two equal-amplitude solitary waves exceeds twice the amplitude of the incident solitary wave. Su & Mirie (1980) carried out a comprehensive perturbation analysis for the head-on collision of two arbitrary-amplitude solitary waves to third order. They derived the maximum amplitude of the head-on collision to be

$$\varepsilon_{max} = \varepsilon_R + \varepsilon_L + \frac{\varepsilon_R\,\varepsilon_L}{2} + \frac{3}{8}\varepsilon_R\,\varepsilon_L(\varepsilon_R + \varepsilon_L), \tag{2.1}$$

where $\varepsilon_{max} = a_{max}/h_0$ represents the maximum amplitude during the collision process, and $\varepsilon_L = a_L/h_0$ and $\varepsilon_R = a_R/h_0$ are normalized individual wave amplitudes in which the subscript L denotes the left-running wave and R the right-running wave. A head-on

collision leaves imprints on the colliding waves with phase shifts, which means the trajectory of each solitary wave in the x–t plane is not the same before and after the collision. Contrary to the 'strong' interaction of solitary waves, a head-on collision causes retardation in phase. According to Su & Mirie (1980), the phase shifts of the right-running wave and the left-running wave are, respectively:

$$\left.\begin{aligned}\Delta\theta_R &= h_0\left(\frac{\varepsilon_L}{3}\right)^{1/2}\left(1+\frac{\varepsilon_L}{8}+\frac{3\varepsilon_R}{4}\right),\\ \Delta\theta_L &= -h_0\left(\frac{\varepsilon_R}{3}\right)^{1/2}\left(1+\frac{\varepsilon_R}{8}+\frac{3\varepsilon_L}{4}\right).\end{aligned}\right\} \tag{2.2}$$

They further showed that after collision, each solitary waveform becomes asymmetrical and tilts backward with respect to the direction of its propagation. As a result of collision, secondary dispersive waves are generated, which trail the parent waves. They found that the secondary trailing wave can be expressed as:

$$\eta = \gamma SS' - \tfrac{4}{9}\gamma S', \tag{2.3}$$

in which the prime represents the total derivative, and, for the right-running wave,

$$\gamma = 9\varepsilon_R^{3/2}\varepsilon_L^{1/2}, \quad S = \operatorname{sech}^2\tfrac{1}{2}\xi_0, \quad \text{and} \quad \xi_0 = \varepsilon^{1/2}k(x-c_Rt), \tag{2.4a–c}$$

in which k is the wavenumber and c_R is the right-running wave speed. (A similar equation is applicable for the trailing left-running wave.) Su & Mirie (1980) attempted to validate their theoretical predictions with the numerical and laboratory experiments given by Chan & Street (1970) and Maxworthy (1976). (Note that those experimental results are only for the head-on collision of identical solitary waves.) The prediction of the maximum amplitude (2.1) is found to be in agreement with the experimental data, while the prediction of the phase shift (2.2) is significantly different from the experimental data: in fact, the measurements by Maxworthy (1976) show amplitude-independent phase shifts. The nature of the secondary wave (2.3) has not been measured in the laboratory.

Head-on collisions of two identical solitary waves were further investigated by other researchers. Fenton & Rienecker (1982) used the Fourier-series method to solve the fully nonlinear Euler equation, and their results for maximum amplitude at the collisions are in good agreement with the experimental results of Chan & Street (1970). Renouard, Santos & Temperville (1985) found a loss in amplitude as the reflected wave propagates away from the vertical wall in their experiments on solitary wave reflection. (Note that except for the boundary layer effect, wave reflection at a vertical wall is equivalent to the head-on collision of equal-amplitude waves.) Cooker, Weidman & Bale (1997) provided numerical results for the collision of a solitary wave onto a vertical wall, and derived the phase shift indicators, i.e. the attachment, detachment and residence times of the collision, from the third-order results of Su & Mirie (1980). Craig *et al.* (2006) presented a numerical analysis based on a pseudo-spectral method in space, solving the Euler formulation for water-wave problems. Furthermore, Craig *et al.* gave theoretical results for a relationship between the change in amplitude of solitary waves due to collision and the energy carried away from the interaction by the trailing wave trains. They also analysed the size of the trailing waves generated by solitary-wave collisions. Chambarel, Kharif & Touboul (2009) investigated the head-on collision of two equal and two unequal steep

solitary waves numerically by the boundary integral equation method. They found a phenomenon corresponding to the occurrence of a thin residual jet during collision when the normalized amplitude of the two solitary waves exceeds 0.60.

The present laboratory study was designed to validate the theoretical results, primarily, of Su & Mirie (1980) and the numerical results of Craig *et al.* (2006) in terms of wave amplification and phase shift associated with the counter-propagating solitary waves. It is noted that Craig *et al.* also compare their numerical simulations with laboratory data, but only one case was presented.

3. Experiment set up and data analysis

Laboratory experiments were performed in a wave tank, which was designed and constructed for long-wave research. The wave tank is 7.3 m long, 3.6 m wide, 0.3 m deep and elevated 1.2 m above the ground. Figure 1 depicts schematics of the apparatus. The sidewalls as well as the bottom of the tank are made of 12.7 mm thick glass plates to allow the use of optical techniques. The top surface of the entire 3.6 m $\times$ 7.3 m aluminium frame was planed in one piece to achieve a smooth flat surface. With the height-adjustable base columns, the glass plates were directly installed on the frame in a precisely horizontal plane. The wave tank is equipped with a 16-axis wavemaker system installed along the 3.6 m long headwall. This wavemaker system is capable of generating arbitrarily shaped, multi-directional waves. Each wave paddle is pushed through hinge connections by two adjacent linear-motor motion devices: the linear motor is inherently more accurate for producing linear positioning than an ordinary servomotor. Vertical paddles are made of polyvinylidene fluoride plates that are moved horizontally in piston-like motions. The maximum horizontal stroke for each paddle is 55 cm, which is more than sufficient to generate very long waves with the water depth of $h_0 = 6.0$ cm used in our experiments.

In the present study, the origin of the coordinates is taken at the initial wave paddle position as shown in figure 1; the x direction points horizontally along the sidewall, y direction points perpendicularly away from the sidewall and z direction points upwards.

Goring & Raichlen (1980) presented an algorithm for the generation of a solitary wave. The motion of the wave paddle is set to match the depth-averaged fluid velocity; hence the time history of wave-paddle displacement $\xi(t)$ can be determined by

$$\frac{\mathrm{d}\xi(t)}{\mathrm{d}t} = \bar{u}(x = \xi(t), t), \tag{3.1}$$

where $\bar{u}$ is the depth-averaged velocity for finite-amplitude shallow-water waves:

$$\bar{u}(x, t) = \frac{c\eta(x, t)}{h_0 + \eta(x, t)}, \tag{3.2}$$

in which c is the wave speed. For the present study, we use the higher-order solution of solitary waves given by Grimshaw (1971) that is explicitly presented by Tanaka (1993). In non-dimensionalized form, the higher-order solitary wave can be expressed as

$$\eta = a\,s^2 - \tfrac{3}{4}a^2(s^2 - s^4) + a^3\left(\tfrac{5}{8}s^2 - \tfrac{151}{80}s^4 + \tfrac{101}{80}s^6\right), \tag{3.3}$$

with

$$\left.\begin{aligned} s &\equiv \operatorname{sech}\{\alpha(x - F\,t)\}, \\ F &= 1 + \tfrac{1}{2}a - \tfrac{3}{20}a^2 + \tfrac{3}{56}a^3, \\ \alpha &= \sqrt{\tfrac{3}{4}a}\left(1 - \tfrac{5}{8}a + \tfrac{71}{128}a^2\right), \end{aligned}\right\} \tag{3.4}$$

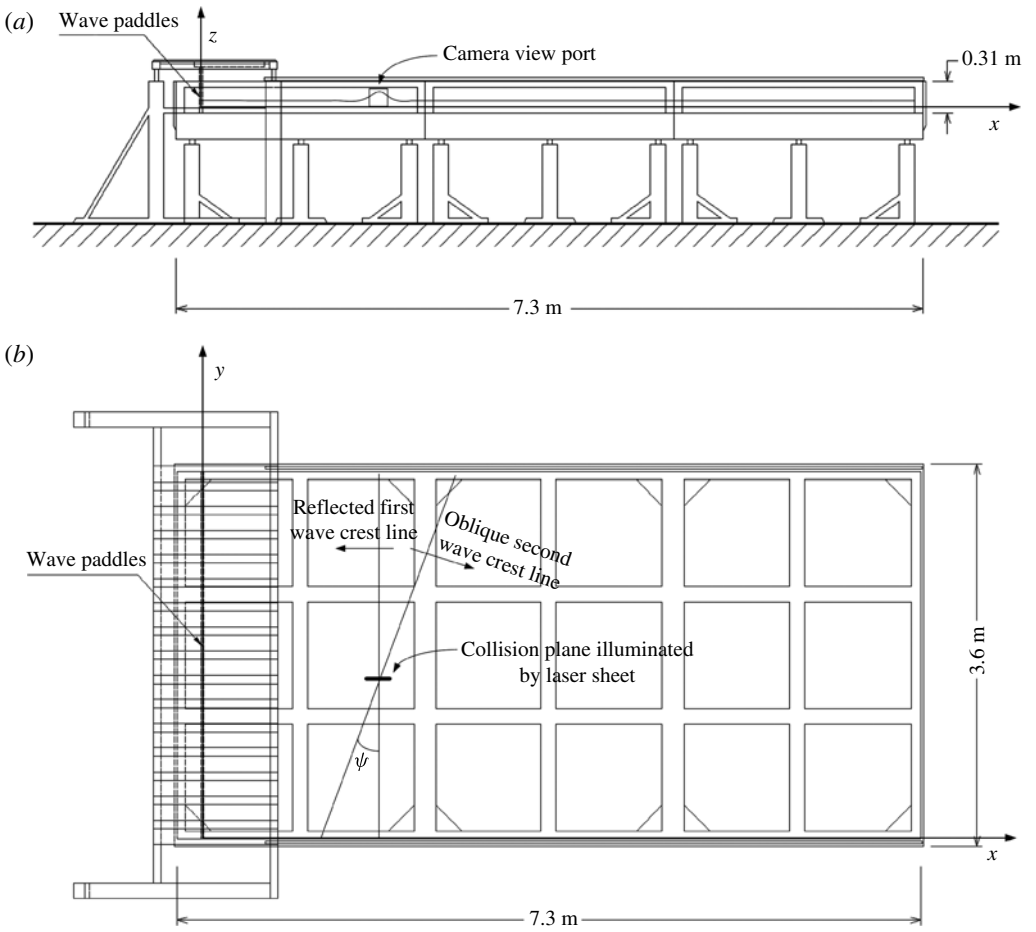

FIGURE 1. Schematic drawings of the wave basin. Elevation view (*a*) showing position of the camera view port. Plane view (*b*) showing the collision of the parallel wave and the oblique wave at an angle ψ. The coordinate system defined in the figure is used to describe the apparatus position.

where the lengths are scaled by the quiescent-water depth h_0 and the time is scaled by h_0/c_0 with $c_0 = \sqrt{gh_0}$: therefore, the wave celerity used in (3.2) is $c = c_0 F$.

For all the laboratory results presented in this paper, the still-water depth is set constant at $h_0 = 6.0$ cm, and hereafter the lengths and time are in the non-dimensionalized form, unless otherwise stated. The following cases were examined:

(i) head-on collision of two waves with equal amplitude travelling in opposite directions; we called this case a 'symmetric head-on' collision for brevity: $\varepsilon = \varepsilon_R = \varepsilon_L$, and $\psi = 0°$ (ψ is the angle between the right-running and left-running wave crests as shown in figure 1);

(ii) head-on collision with unequal amplitudes which we called an 'asymmetric head-on' collision: $\varepsilon_R > \varepsilon_L$, and $\psi = 0°$;

(iii) collision of identical waves intersecting with an oblique angle which we called a 'symmetric oblique' collision: $\varepsilon = \varepsilon_R = \varepsilon_L$, and $\psi = 10°$, 15°, and 20°;

(iv) collision of two waves with unequal amplitudes with an oblique angle which we called an 'asymmetric oblique collision': $\varepsilon_R > \varepsilon_L$, and $\psi = 10°$, 15°, and 20°.

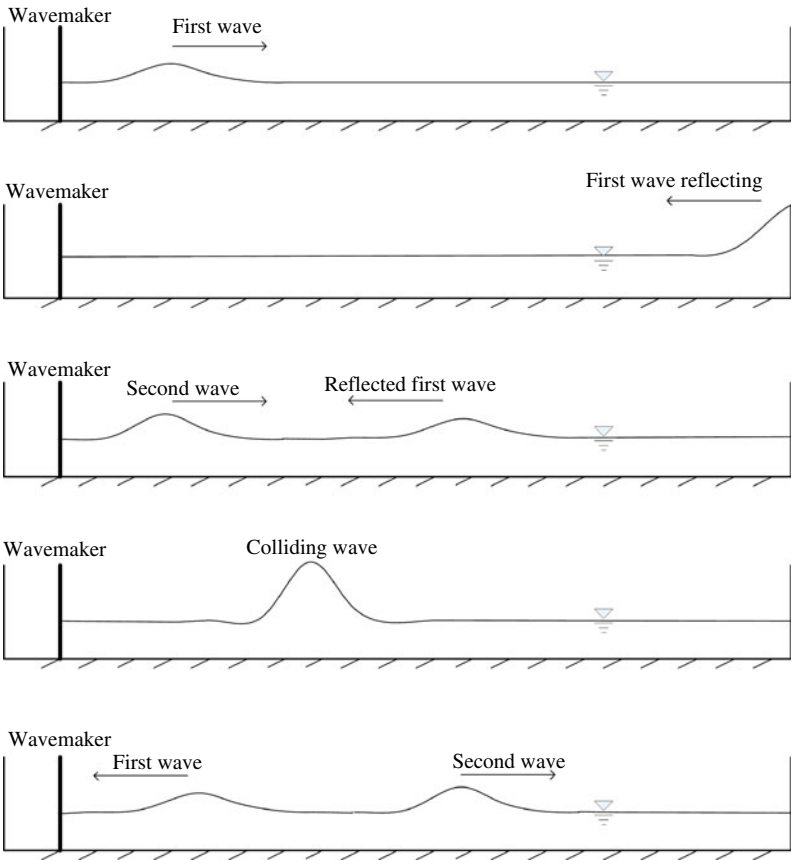

FIGURE 2. Sketch of the procedure for generating two counter-propagating solitary waves.

In the experiments, dual solitary waves were generated in sequence with a certain time in between. As sketched in figure 2, while the first wave is reflected at the endwall and propagates backward toward the wavemaker, the second wave is then generated so that these two waves collide at the specified location. The time interval between these two waves is controlled by the wavemaker control system. For head-on collision cases, waves propagate perpendicular to the wavemaker (in the direction parallel to the sidewalls). For waves with oblique collisions, we generated the first wave perpendicular to the wavemaker, but created the second wave with a specified oblique angle (see figure 1). By controlling the wavemaker motion, these two waves collide each other at the predetermined location that is 1.5 m away from the wave paddles. Given the unavoidable viscous damping effect, a slightly larger amplitude for the first wave was programmed by trial-and-error so that the two waves were practically identical at the collision point.

With the use of four non-contacting capacitance-type wave gauges, Hammack *et al.* (2004) repeated an identical experimental run 40 times to capture the solitary wave collision process with a spatial resolution of 1 cm in a propagation span of 1.6 m. Note that wave-gauge measurement depends on calibrating it under the quiescent condition (i.e. static calibration). Their measurement procedure – repeating an experimental run 40 times – requires precise repeatability and stability in instrumentation. Although the still-water level was carefully monitored and adjusted

during the repeated runs, the measurement involves uncertainties associated with the instrumentation. In the present study, the laser-induced-fluorescent (LIF) imagery method is used to study temporal and spatial variations of water-surface profiles: note that the LIF method was used to record water-surface variations of bores as early as 1980s (Yeh & Ghazali 1986; Ramsden 1993; Duncan *et al.* 1994), and to capture the detailed incipient wave-breaking process (Duncan *et al.* 1999; Liu & Duncan 2006; Diorio, Liu & Duncan 2009). In this method, a laser beam is converted to a thin laser sheet using a cylindrical lens. With the aid of fluorescein dye dissolved in water, the vertical laser-sheet illumination from above induces the dyed water to fluoresce and identifies a water-surface profile directly and non-intrusively. The illuminated images were recorded with a high-speed high-resolution video camera. Captured images from the perspective view are transformed to orthographic view with the aid of the calibration image, mapping the obtained data into physical dimension units, so that the resulting images can be analysed quantitatively. The transparent glass bed of the tank minimizes the reflection of laser illumination that could have caused noise in the wave-profile images.

In the data processing, image pixels are traced in the vertical direction from top to bottom. The air–water surface is determined by where the gradient of the light intensity reaches a maximum. Note that the measurement plane is sufficiently far away from the sidewall to prevent sidewall influence on the measurement section. Unlike capillary waves or breaking waves, long waves have an inherently small vertical-to-horizontal ratio. Our laboratory experiments require measurements of small wave amplitudes (1.0–3.2 cm) in a large horizontal span (approximately 1 m). Consequently, one of the difficulties for the LIF method is resolution. To overcome this, we used a montage method. Taking advantage of the highly precise repeatability of our experimental apparatus, the LIF water-surface profiles were measured on five connected panels, each a 27 cm segment, making profiles approximately 1.3 m long. Note that with the use of the CCD camera (1280 pixels $\times$ 1024 pixels), the resulting vertical resolution is better than 0.15 mm. A similar montaging technique was used by Li, Yeh & Kodama (2011) for their experiments on Mach reflection of solitary waves.

Another difficulty in the laboratory experiments was associated with the cases of oblique collision. Due to the finite width of the wave tank, the collision site must be located to avoid the sidewall effects. We found the optimum site to be at ($x =$ 1.5 m, $y = 1.3$ m), avoiding the energy leakage due to diffraction from the sidewall ($y = 3.6$ m) and energy reflection from the opposite sidewall ($y = 0$). Because of the sidewall effects – wave reflection and diffraction – the oblique angle is limited to be less than 20°, although the wavemaker itself is capable of generating waves with oblique angle of 45°. Note that our precisely controlled wave generation system allowed us to study the collision process in the area relatively near the wavemaker: $x/h_0 \approx 26$.

4. Results

Figure 3 shows the spatio-temporal water-surface profile obtained with the LIF technique. The counter-propagating waves both have amplitude $\varepsilon = a/h_0 = 0.40$ prior to the collision: it is a symmetric head-on collision with $\psi = 0°$. A small phase shift before and after the collision can be seen by tracing each wave-crest trajectory in the figure. Note that trailing small waves are generated after the collision. Also recall that we used the montage method to patch five panels together: hence there are slightly visible vertical strips (for example at the location around $x/h_0 = 21.5$) in figure 3.

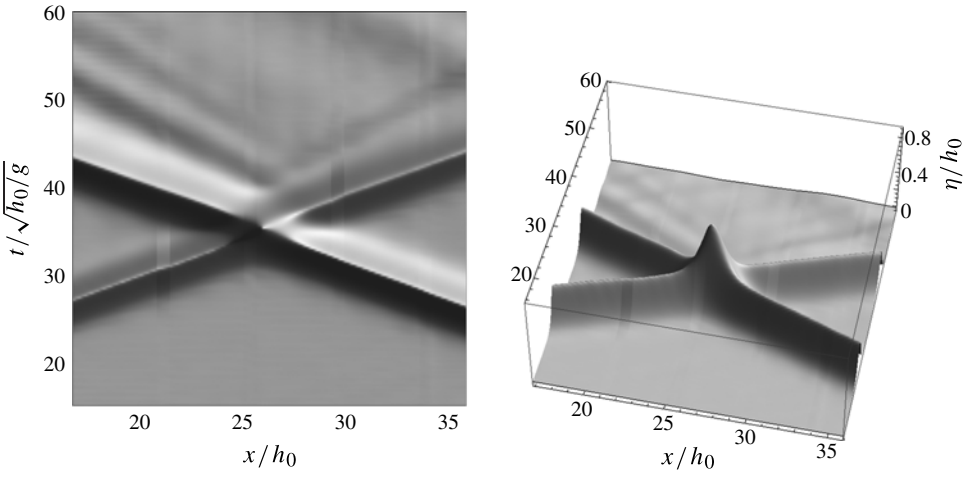

FIGURE 3. Two views of temporal variation of the water-surface profile in the x–z plane (parallel to the sidewall). The water depth $h_0 = 6.0$ cm. The colliding waves are of equal amplitude $\varepsilon_R = \varepsilon_L = 0.40$. The data were obtained with the LIF method.

Figure 4 compares snapshots of the collision process, extracted from the water-surface profiles presented in figure 3, together with the linear superposition of two counter-propagating KdV soliton profiles for comparison. The time origin is set at the moment of the maximum amplitude, so negative time means before the collision and positive time means after the collision. Note that the soliton profiles were fitted to the experimental wave profiles at $t = -0.58$ s, well before the collision. When $t = -0.21$ s, the two waves start elevating the water surface by interaction. At $t = -0.05$ s, the linear superposition of KdV solitons peaks ($\varepsilon = 0.80$), while the experimental data show that the two waves are still climbing until $t = 0$ s. The wave profile at $t = -0.05$ s is very close to that of the linear superposition of the two solitary waves. Evidently, the phase lag must result from this extra runup process beyond the linear superposition. The water surface peaks at $\varepsilon_{max} = 0.902$, which is 12.8 % higher than linear superposition of the two incident wave amplitudes. The theoretical prediction (2.1) yields $\varepsilon_{max} = 0.928$ for $\varepsilon = 0.40$, which is slightly higher (2.9 %) than the measurement but considered in good agreement. After peaking, the water level starts to fall. When $t = 0.14$ s, the two waves start to separate from each other. There is an apparent phase difference between the linear superposition and the experimental result. At $t = 0.48$ s, the spatial profile of each wave becomes asymmetrical, tilting slightly backward with respect to the direction of its propagation. During $t = 0.48$–0.79 s, two small humps appear that start to trail each solitary wave. The tilting wave profile, as well as the trailing small waves, will be discussed in detail later. All the foregoing collision behaviours are in accord with the theoretical predictions of Su & Mirie (1980), as well as the numerical results of Craig *et al.* (2006).

The amplitude variations of the left- and right-running waves are plotted in figure 5(*a*). After collision, the amplitude of each wave decreases. Our results show practically equal amplitude reduction for the left-running wave (−6.62 %) and right-running wave (−6.67 %), reflecting the symmetric nature of the collision. To compare the measured amplitude variation with the numerical simulation of the Euler model given by Craig *et al.* (2006), the temporal variation of the amplitude is plotted in figure 5(*b*). The agreement is excellent, although the slightly lower

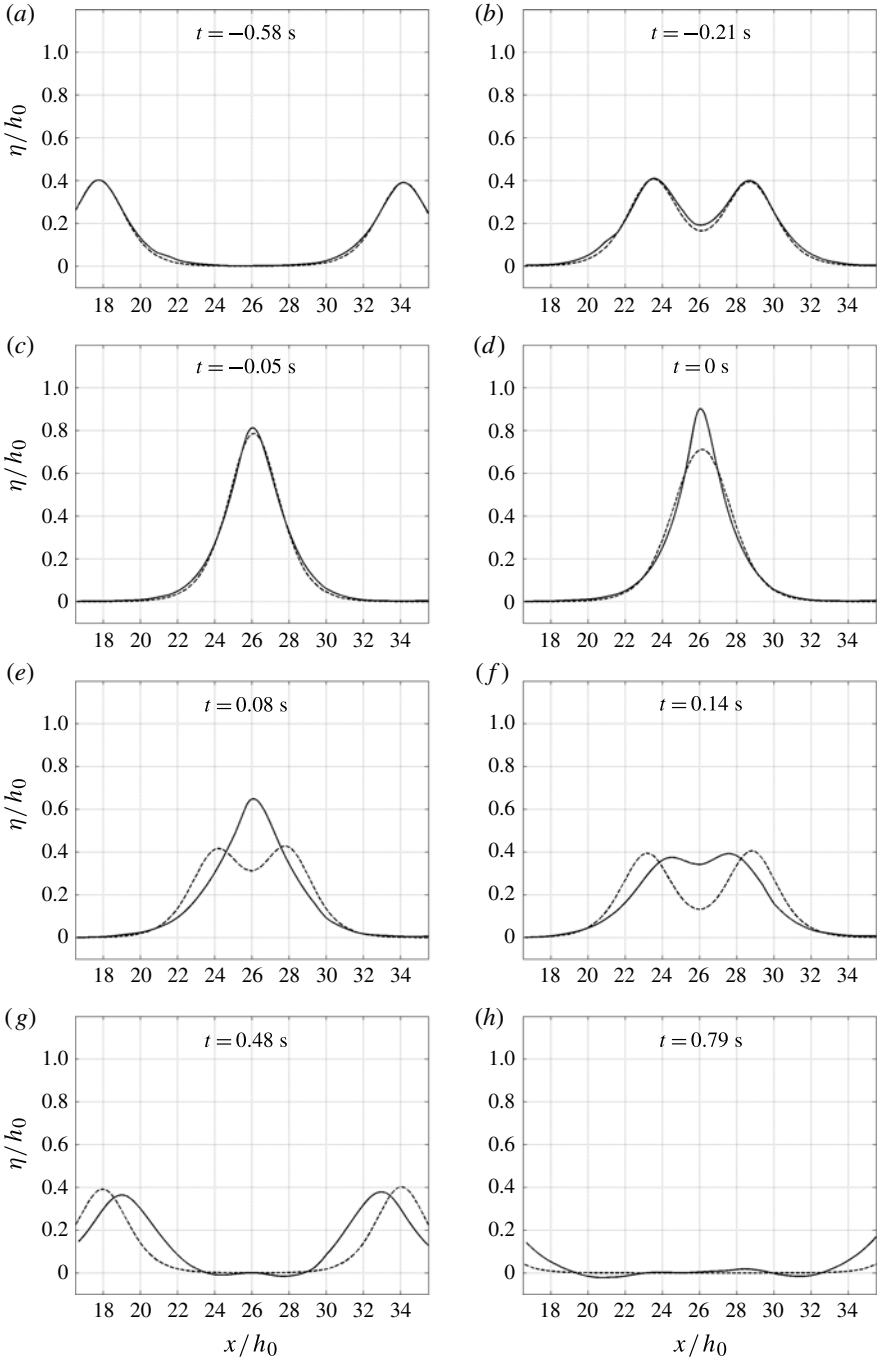

FIGURE 4. Water-surface profile during symmetric head-on collision of two solitary waves with height $\varepsilon_R = \varepsilon_L = 0.40$: ———, experimental data; – – – – –, linear superposition of the counter-propagating KdV solitons.

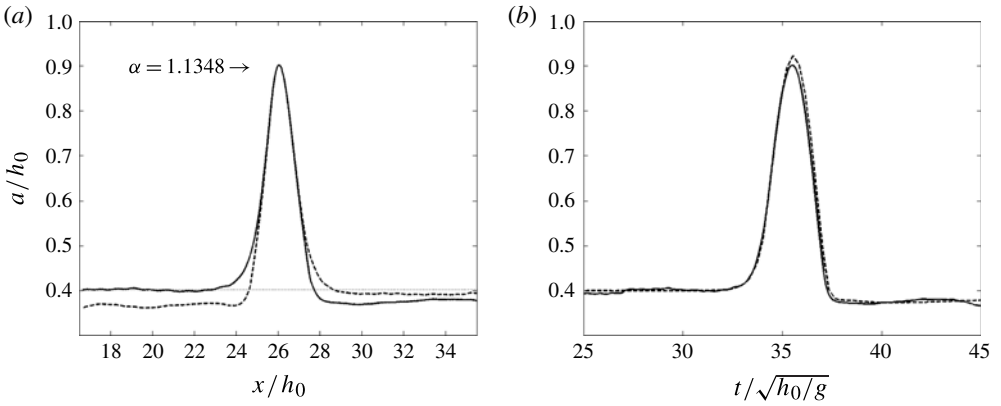

FIGURE 5. (*a*) Amplitude of the right-running (———) and left-running wave (– – – – –) at the location of symmetric head-on collision ($\alpha = 1.1348$ is maximum amplification over linear superposition of the two incident waves); (*b*) temporal variation of the measured maximum amplitude (———) in comparison with the numerical simulation (– – – – –) given by Craig *et al.* (2006). Here $\varepsilon_R = \varepsilon_L = 0.40$.

maximum amplitude in the experiment is a result of dissipation and surface tension effects of the real fluid, which is expected.

The phase shift caused by the collision is obtained as follows. The wave-crest trajectory is assumed to be asymptotic to the line $x = c_j t + a_j$ before collision and $x = c_j^+ t + a_j^+$ after collision, in which the subscript $j = (R, L)$ denotes the right-running and left-running solitary waves, respectively. The midpoint of the interaction is defined as the time τ. The phase shift $\Delta\theta$ in the laboratory data is calculated by the difference in the intercept of the asymptotic lines at $t = \tau$: $\Delta\theta = (a_j^+ - a_j) + \tau(c_j^+ - c_j)$. Note that Craig *et al.* (2006) used this method to determine the phase shift. Figure 6 shows the space–time trace of the local maximum (wave crest) of the experimental data of figure 3 as the two individual crests merge and then separate; also plotted is the numerical result from Craig *et al.* (2006). Excellent agreement of the measured phase shift with the numerical simulation is evident. The measured phase shift for the right-running wave is $\Delta\theta_R/h_0 = 0.98$, while the shift for the left-running wave is $\Delta\theta_L/h_0 = 1.1$. On the other hand, the shift predicted by (2.2) is 0.49, which is not in agreement. Such a discrepancy was also reported by Su & Mirie (1980), who made the comparison of their prediction (2.2) with Maxworthy's (1976) laboratory data. The discrepancy in phase shift must result from an ambiguity in defining the phase shift from the measured water-surface profiles. Immediately after the collision, the wave profile becomes asymmetric, tilting backward with respect to the direction of its propagation. Consequently, the phase shift based on the wave-crest trajectory yields a larger shift than the asymptotic value of (2.2). Our laboratory measurements were taken following the wave-crest trajectory along a span of approximately 100 cm. The colliding solitary waves lose amplitude after collision, hence their propagation speed is slowed. This transient collision behaviour also makes defining the phase shift difficult.

Fenton & Rienecker (1982) showed in their numerical analysis that the spatial phase shift is very sensitive to the distance from the collision location. They compared their numerical results with the two phase-shift limits from Su & Mirie (1980): one is for

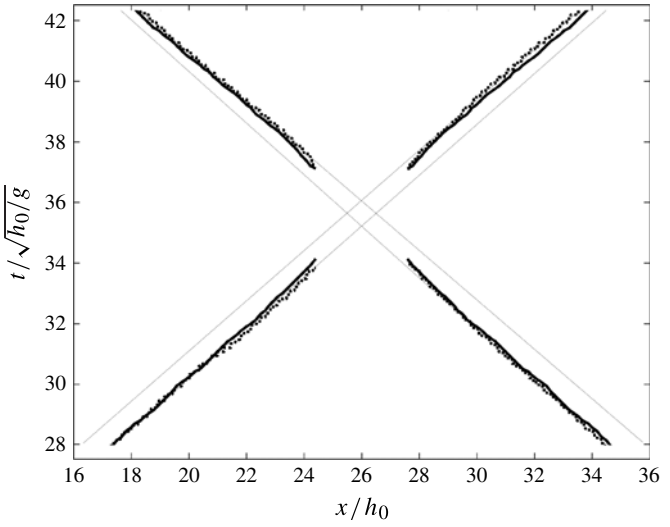

FIGURE 6. Wave-crest trajectory of symmetric head-on collision of two solitary waves of equal height $\varepsilon = 0.40$. Solid lines represent the measured wave crest trajectory; dotted lines represent the crest trajectory of the numerical prediction (Craig *et al.* 2006). The thin lines represent traces of the left- and right-running wave crests before and after collision extracted from the simulation.

the asymptotic shift given in (2.2) representing the phase shift after a long time, and the other is for immediately after the collision:

$$\left.\begin{aligned} \Delta\theta_R/h_0 &= \left(\frac{\varepsilon_L}{3}\right)^{1/2}\left(1+\frac{\varepsilon_L}{8}+\frac{23\varepsilon_R}{4}\right), \\ \Delta\theta_L/h_0 &= -\left(\frac{\varepsilon_R}{3}\right)^{1/2}\left(1+\frac{\varepsilon_R}{8}+\frac{23\varepsilon_L}{4}\right). \end{aligned}\right\} \tag{4.1}$$

For $\varepsilon_L = \varepsilon_R = 0.40$, (4.1) yields the phase shift $\Delta\theta/h_0 = 1.22$, which is in better agreement with both the results of our laboratory measurements and the numerical simulation by Craig *et al.* (2006).

Figure 7 shows waterfall plots of the collision process, presenting the runup motion ($t < 0$) that overshoots the linear superposition, and the subsequent rundown motion ($t > 0$) that penetrates below the still-water level. Figure 8(*a*) presents a time sequence of the rundown motion leading to the penetration. The process shown in the figure suggests that this disturbance from penetration is responsible for creating the dispersive trailing wavetrain as shown in figure 8(*b*). The measured dispersive wavetrain is compared in figure 8(*b*) with the theoretical prediction (2.3). Considering its very small and transient waves, the measured wave amplitudes and wavelengths in the laboratory are in good agreement with theory.

Figure 9 shows a snapshot of the wave profile after the collision ($t = 0.35$ s), demonstrating the backward-tilting profile formation in both departing waves; the tilting behaviour is predicted by Su & Mirie (1980) as discussed earlier. To see the asymmetric profile explicitly, the linear superposition of two KdV solitons is depicted on the figure, positioning their crests at the corresponding waves. The tilt in the right-departing wave is evident, as is that in the left-running wave but with a

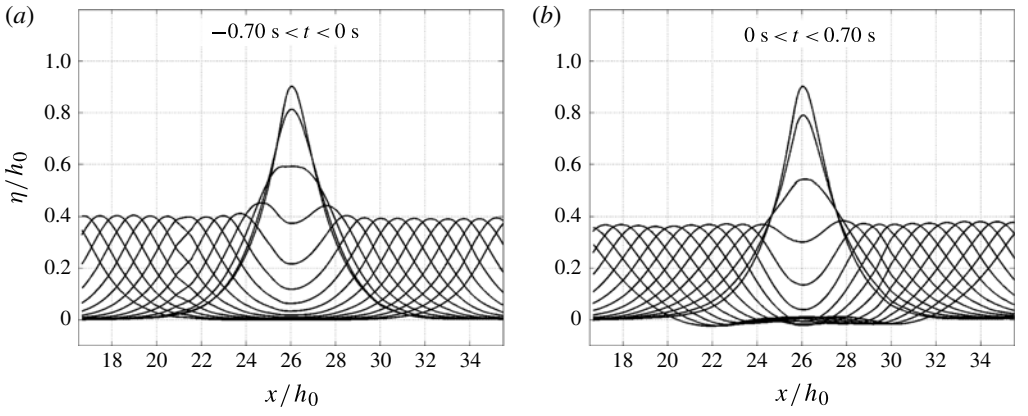

FIGURE 7. Waterfall plots of the temporal variation of the water-surface profile for $\varepsilon_L = \varepsilon_R = 0.4$: (*a*) before the collision for 0.7 s; (*b*) after the collision for 0.7 s. The time interval of the profiles is $\Delta t = 0.05$ s.

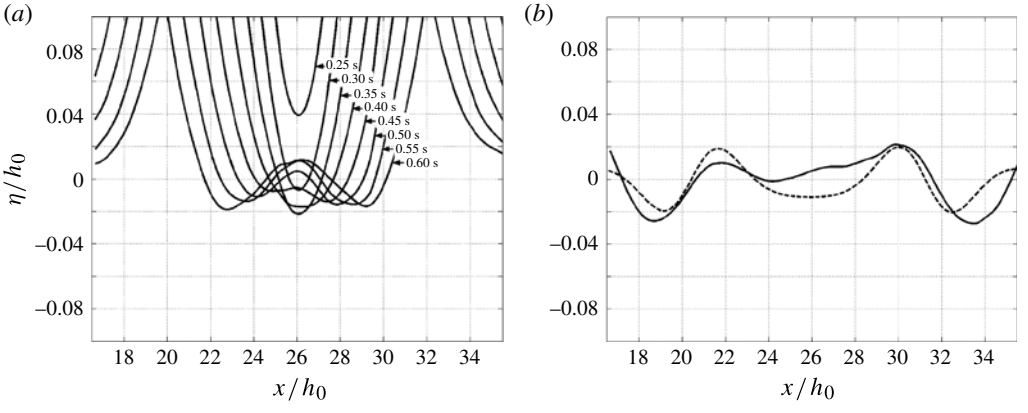

FIGURE 8. (*a*) Time sequence of the detailed rundown motion for $\varepsilon_R = \varepsilon_L = 0.40$ that penetrates below the still-water level; (*b*) comparison of the measured dispersive trailing wavetrain (———) with the theoretical prediction (– – – – –) by (2.3) at $t = 0.96$ s.

smaller tilt. Also note that the measured wave profile immediately after the collision is broader than that of the KdV soliton.

Figure 10 shows the symmetric head-on collision for the highest waves that we could produce. Recall that our experimental procedure is to generate one of the colliding waves by reflection at the endwall of the wave tank. This limits the highest wave, because of the amplitude attenuation by the time it comes back to the collision site. We could not produce any case with $\varepsilon_L = \varepsilon_R > 0.60$, for which Chambarel *et al.* (2009) claimed that a thin residual jet will form. The maximum wave amplitude prior to the collision we were capable of obtaining is $\varepsilon_L = \varepsilon_R = 0.52$.

Figure 10 shows that the collision runup and rundown processes are different. In the runup process, the colliding waves gradually merge, increasing their amplitudes; the inflection point of the water-surface profile occurs at $\eta/h_0 \approx 0.7$. The rundown process, on the other hand, shows that the inflection point occurs at $\eta/h_0 \approx 0.50$. The time-lapse profiles in figure 10(b) also show the formation of nodes around $\eta/h_0 \approx 0.45$

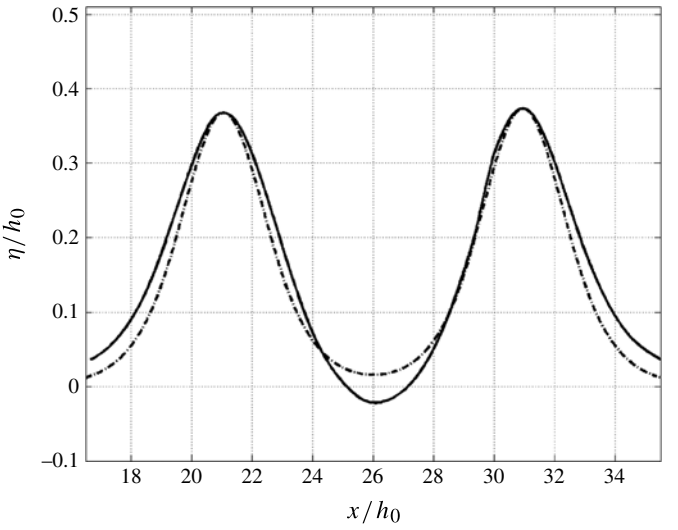

FIGURE 9. Water-surface profile after symmetric head-on collision of two solitary waves, $t = 0.35$ s, with height $\varepsilon_R = \varepsilon_L = 0.40$: ———, experimental data; –·–·–, linear superposition of the KdV solitons positioned at the wave crests. The measured wave profiles are tilted backward.

during the rundown process. Also observed is that the amplitude of each departing wave momentarily becomes smaller than that of the subsequently formed outgoing waves.

Figure 11 shows the measured amplitudes for symmetric head-on collisions together with the theoretical prediction (2.1) and the previous numerical and experimental data. The present laboratory results are in excellent agreement with the theoretical and numerical predictions. It is also observed that the present measurements are in better agreement than the laboratory data provided by Maxworthy (1976).

Maxworthy performed his laboratory experiments in a flume 5 m long, 20 cm wide and 30 cm deep, with the water depth $h_0 = 4.5$–6.7 cm. He conducted two different experiments: (i) examining wave reflection at the tank endwall, and (ii) wave–wave interaction by generating the same wave from each end of the tank. For the former case, the initial wave generation was done by manually moving a vertical plate, utilizing the dispersive characteristic to generate a leading solitary wave within a sufficient propagation distance. For the latter case, he installed a movable partition gate at each end and generated two counter-propagating waves by lifting the gates simultaneously. The propagation distance for this case is one-half the former case because of the collision location at the middle of the tank. Maxworthy's (1976) data for amplitude of the wave reflection at the endwall are in good agreement with the theoretical prediction. On the other hand, the data for his wave–wave collision at the middle of the tank exhibit approximately 10 % greater amplitude than the predictions. It is speculated that this discrepancy could be attributed to the lack of sufficient propagation distance for clean solitary waves to emerge prior to the collision.

The phase-shift data resulting from the head-on symmetric collisions are plotted in figure 12, together with the previous laboratory data (Maxworthy 1976), the theoretical predictions for the asymptotic shift (2.2) and the phase shift at the collision (4.1). Su & Mirie (1980) commented in their analysis that their theory (2.2) cannot account for Maxworthy's experimental results for the phase shift that appear to be

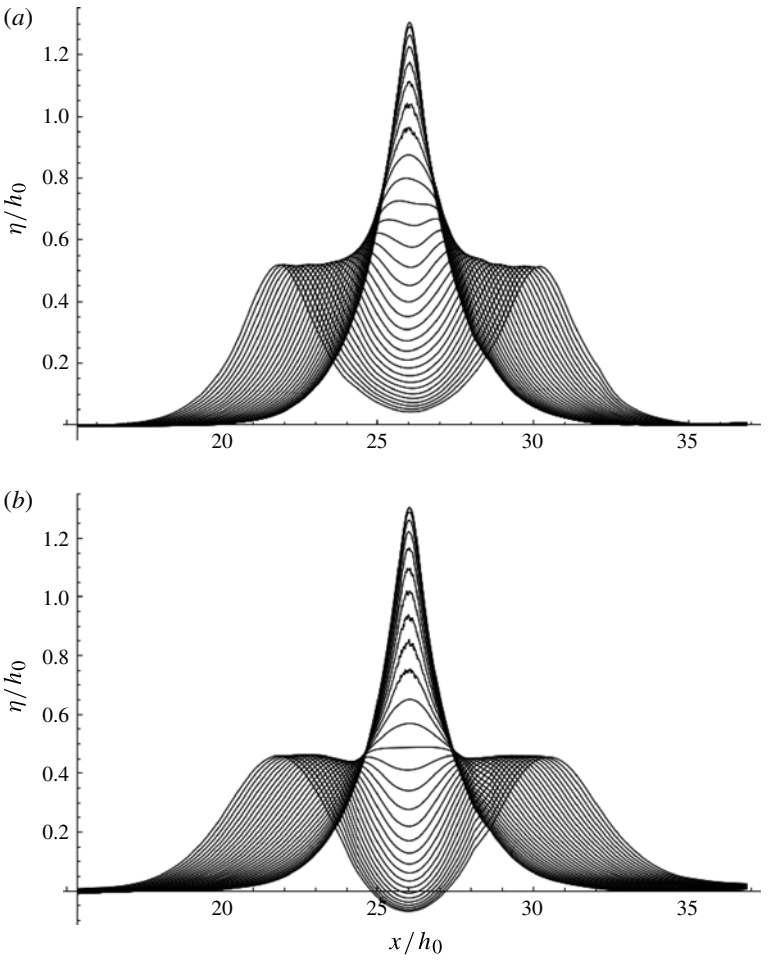

FIGURE 10. Waterfall plots of the temporal variation of the water-surface profile for $\varepsilon_L = \varepsilon_R = 0.52$: (*a*) before the collision for 0.3 s; (*b*) after the collision for 0.3 s. The time interval of the profiles is $\Delta t = 0.01$ s.

amplitude-independent. The present laboratory results show otherwise: there is a clear dependence on wave amplitude, and our laboratory results are in fair agreement with the prediction (4.1). The reason for Maxworthy's laboratory data being independent of the wave amplitude is not clear. It is noted that Maxworthy performed his experiments using the equipment available at that time. As discussed, to study wave reflection at the endwall, a solitary wave was generated by pushing a plate manually in a narrow tank. To study the wave–wave collisions, Maxworthy created the counter-propagating waves by removing a vertical partition to release excess water at each end of the tank. His wave-generation method relied on the dispersive effect in the propagation distance to the collision. Consequently, the lee side of the emerging leading solitary wave could have been contaminated with unwanted trailing noise, and the lee-side condition is crucial to measure the phase shift accurately. It must be emphasized, however, that Maxworthy's crude but cleverly designed experiments provided a good dataset of the maximum wave amplification at the vertical reflective endwall of the

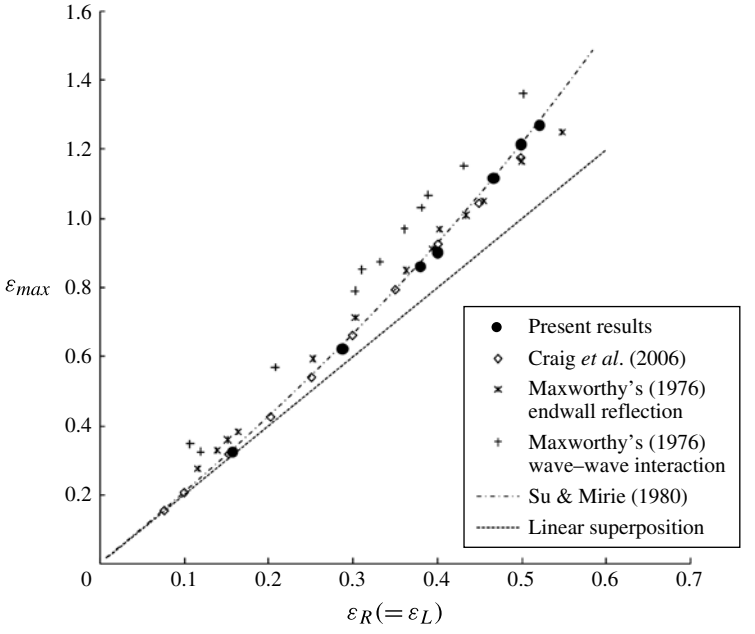

FIGURE 11. Maximum amplitudes of symmetric head-on collisions of solitary waves.

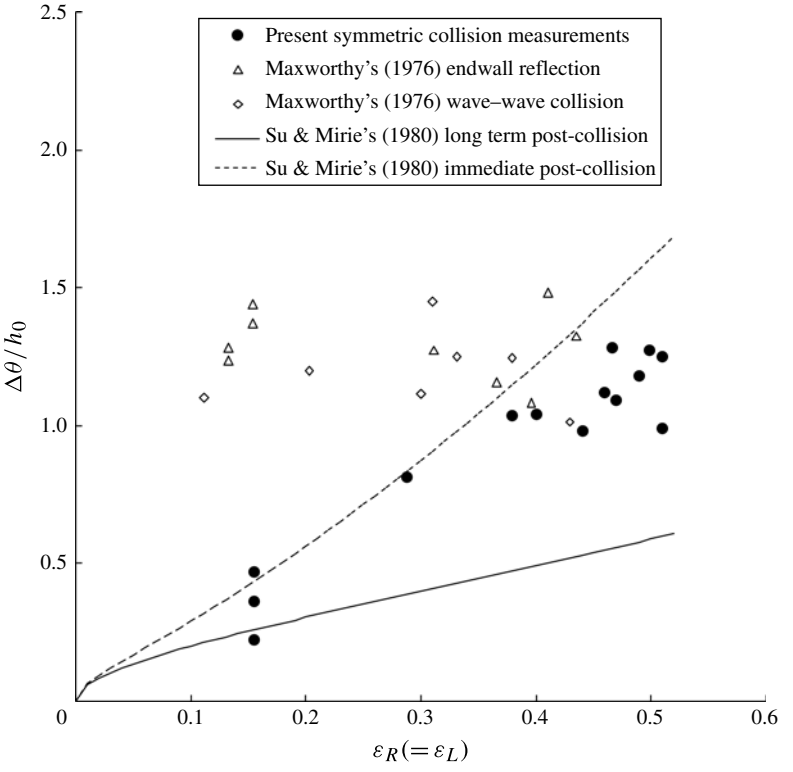

FIGURE 12. Phase shift $\Delta\theta$ versus wave amplitude ε for symmetric head-on collisions of solitary waves: ———, asymptotic value of phase shift (2.2); – – – – –, phase shift immediately after the collision (4.1); symbols show the present measurements and Maxworthy's (1976) experimental results.

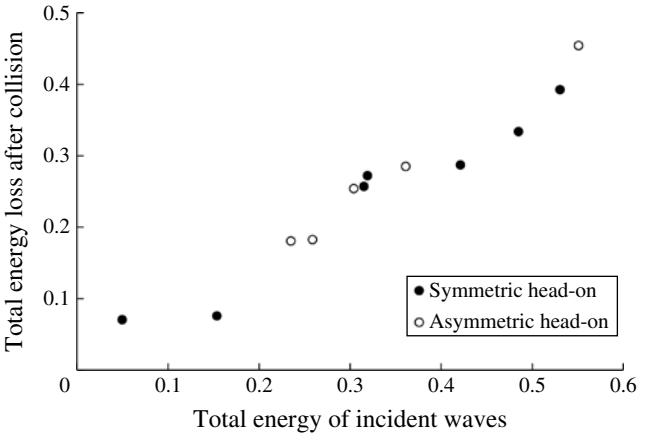

FIGURE 13. Pre-collision total wave energy $\varepsilon_L^2 + \varepsilon_R^2$ versus the energy loss by collision: $(\varepsilon_L^2 - \varepsilon_L'^2)/\varepsilon_L^2 + (\varepsilon_R^2 - \varepsilon_R'^2)/\varepsilon_R^2$ where ε' is the wave amplitude after collision.

tank as shown in figure 11. On the other hand, good measurement of the wave phase requires a more precise apparatus and procedure.

As demonstrated in figure 5, the amplitudes of the post-collision outgoing waves are smaller than the amplitudes of the pre-collision waves. In figure 13, the parameter $\varepsilon_L^2 + \varepsilon_R^2$ that represents the total wave energy prior to collision is plotted versus the energy loss in the separating waves after collision: $(\varepsilon_L^2 - \varepsilon_L'^2)/\varepsilon_L^2 + (\varepsilon_R^2 - \varepsilon_R'^2)/\varepsilon_R^2$ in which ε' is the wave amplitude after collision. The monotonic relation shown in the figure indicates that the energy loss (i.e. amplitude reduction) is greater for the greater pre-collision waves. The reduction of the wave energy must be attributed to the energy transfer to the generation of trailing wavetrain. The very good agreement in figure 5(*b*) between the measured amplitude and the predicted amplitude based on the Euler model indicated that viscous energy dissipation must be insignificant.

In addition to symmetric head-on collisions, we studied asymmetric head-on collisions, symmetric oblique collisions and asymmetric oblique collisions. Typical results are shown in figure 14. The phase shift and secondary dispersive trailing waves were observed for all cases. Because the interaction of two counter-propagating solitons is 'weak', our laboratory data indicate that the oblique angle apparently does not affect the collision process: we see no significant difference in the wave patterns of figures 3 and 14(*b*) for the symmetric cases, and figures 14(*a*) and 14(*c*) for the asymmetric cases.

Figure 15 compares measured and theoretical maximum amplifications for head-on collisions with equal and unequal amplitudes and also the collisions with oblique angles. Note that amplifications are presented as the ratio of the measured value to the linear superposition of the two colliding waves. Figure 15 indicates that the experimental results agree well with theoretical predictions even though the theory was developed for the head-on collisions only: oblique collisions are not considered in the theory. It must be recalled that the oblique collisions that we examine are those with oblique angles less than 20° because of the limitation of the laboratory basin width as discussed earlier.

The phase shift resulting from a variety of soliton collisions is compared with the theoretical prediction of (4.1) in figure 16. Again, the theory (4.1) is only for normal head-on collisions, not for oblique collisions. Note that (4.1) does not represent the

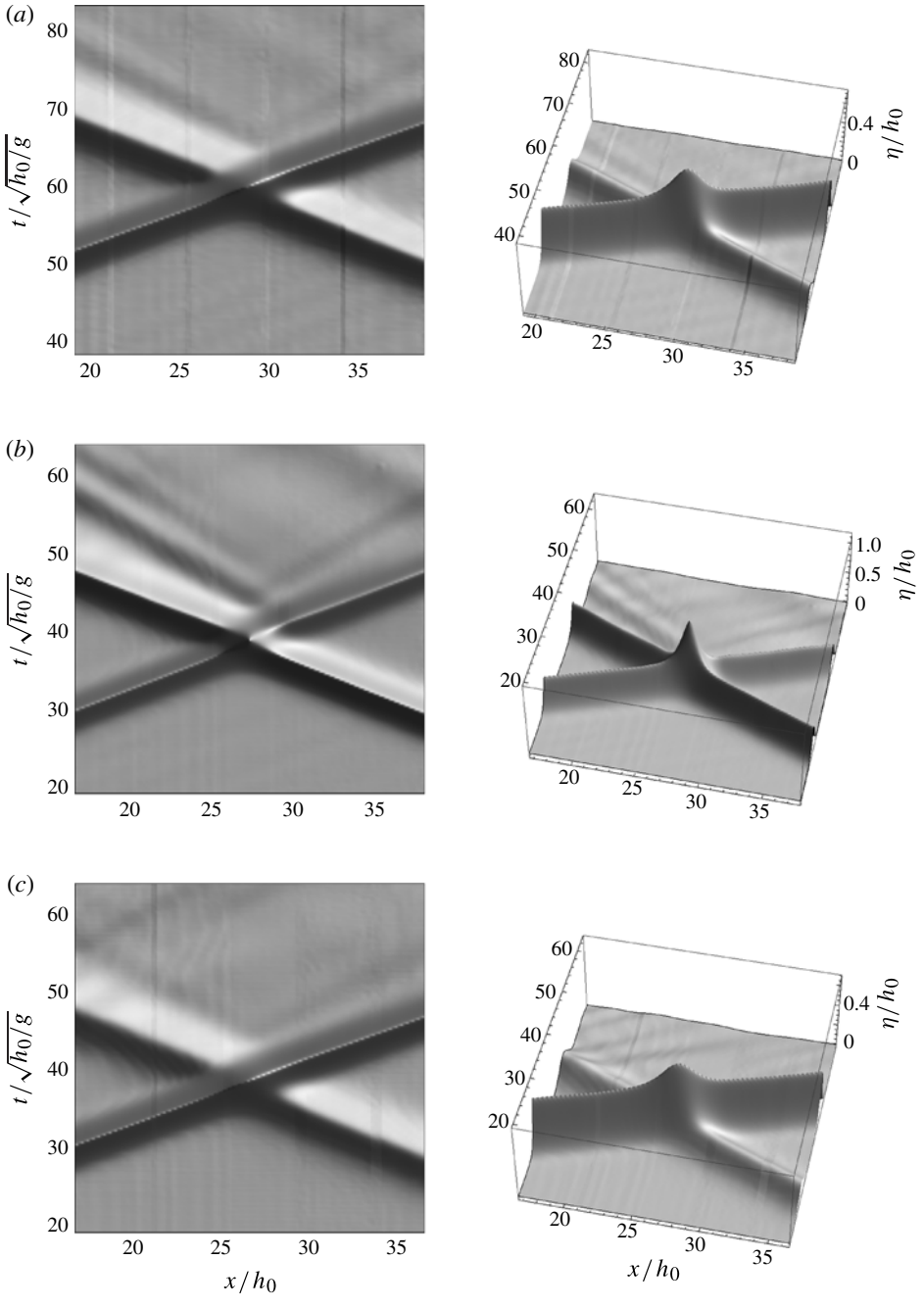

FIGURE 14. Two views of temporal–spatial variations of the colliding water-surface profiles in the x–z plane, obtained by the LIF method. Water depth $h_0 = 6.0$ cm. (*a*) $\varepsilon_R = 0.47,\ \varepsilon_L = 0.19,\ \psi = 0°$; (*b*) $\varepsilon_R = \varepsilon_L = 0.47,\ \psi = 10°$; (*c*) $\varepsilon_R = 0.49,\ \varepsilon_L = 0.15,\ \psi = 10°$.

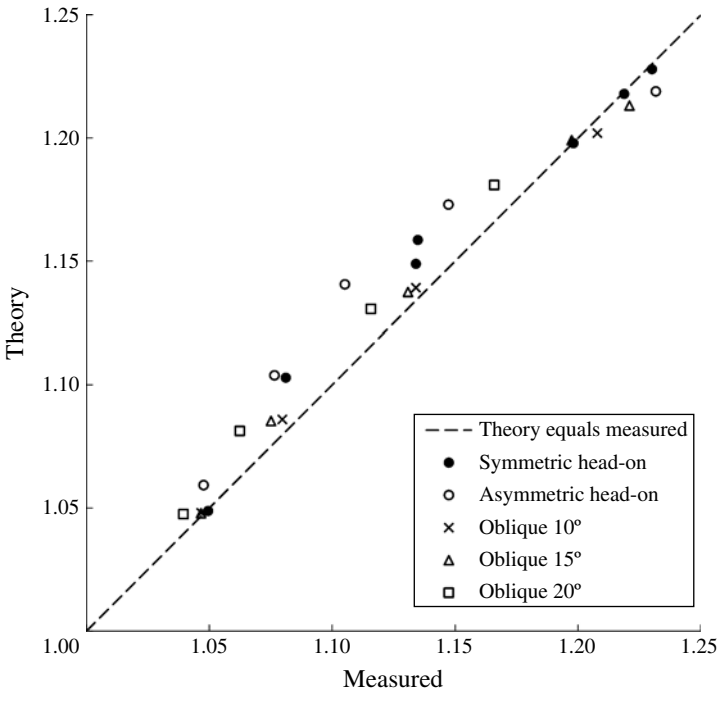

FIGURE 15. Measured maximum amplification $\varepsilon_{max}/(\varepsilon_L + \varepsilon_R)$ versus the prediction (2.1) by Su & Mirie (1980). Value obtained from the maximum amplitude divided by the linear superposition of the amplitude of the two colliding waves.

asymptotic phase shift (2.2) but rather the shift immediately after the collision. In spite of the uncertainty in interpretation of the transient behaviour of the phase shift, figure 16 shows fair agreement with theory (4.1), including the cases of oblique collisions.

5. Summary and conclusions

A series of laboratory experiments were performed to study the collision phenomena of dual counter-propagating solitary waves. The experiments were conducted for a variety of collision conditions, including symmetric head-on, asymmetric head-on, symmetric oblique, and asymmetric oblique collisions. The laser-induced-fluorescent (LIF) technique was used to capture the water-surface variations in space and time.

During the collision, the maximum wave amplitude exceeds that calculated by superposition of the incident solitary waves, and the measured amplitude agrees well with the prediction of the nonlinear theory (2.1) by Su & Mirie (1980). The collision causes attenuation in wave amplitude: the larger the wave, the more the relative amplitude reduction. Judging from the excellent agreement between the present laboratory measurements and the predictions of the Euler model (Craig *et al.* 2006), this amplitude reduction must be related to the energy transfer to the generation of secondary trailing dispersive waves.

The collision also causes phase shifts in the interacting waves. Maxworthy's (1976) experimental results show that the phase shift is independent of incident wave amplitude, which disagrees with Su & Mirie's (1980) theoretical prediction. On the

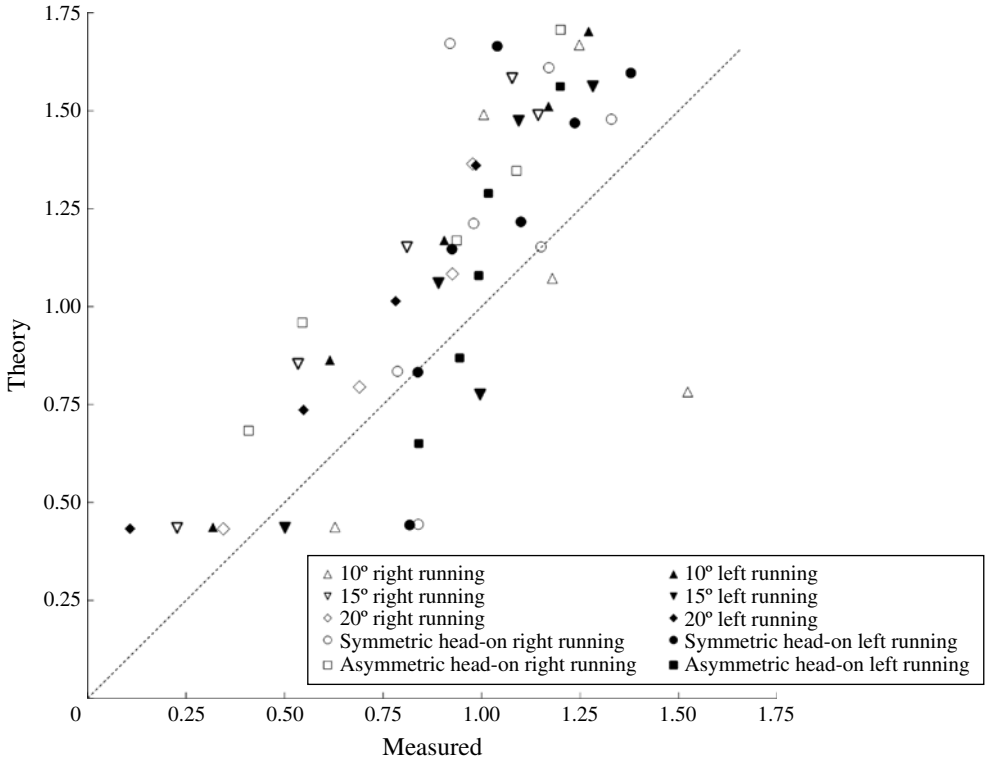

FIGURE 16. Measured phase shift $\Delta\theta_R/h_0$ and $\Delta\theta_L/h_0$ versus the third-order prediction (4.1). The dotted line shows theory equal to measured values.

contrary, the present laboratory results show the dependence on wave amplitude, which agrees with Su & Mirie's prediction (4.1). The secondary dispersive wavetrain resulting from solitary wave collision is compared with (2.3). In spite of its very small and transient wave characteristics, the laboratory observations of the wave amplitude and length agree well with the theory.

We also investigated the symmetric head-on collisions of the highest waves possible in our laboratory, and found that the runup and rundown process is not symmetric. There is penetration of the rundown motion below the still-water level: this penetration results in departing post-collision waves with an asymmetrical waveform with each wave tilting slightly backward with respect to the direction of its propagation. The penetration further causes the generation of the secondary dispersive waves. In this study, we could not generate a collision of two incident waves larger than $\varepsilon = 0.60$: therefore we could not confirm the thin residual jet phenomenon claimed by Chambarel *et al.* (2009).

Su & Mirie's (1980) theory was developed for head-on collisions, while our laboratory results include oblique collisions. The oblique collision cases that we investigated are those with small oblique angles (up to 20°). It was found that the theory serves well for oblique collisions at small angles, which suggests that the obliqueness of the collision may not be important for this 'weak' interaction process.

Acknowledgements

We thank P. Guyenne for providing the numerical data presented in Craig *et al.* (2006). We also thank P. Sollins for his comments and editing. This work was supported by Oregon Sea Grant Program (NA06OAR4170010-NB154L and NA10OAR4170059-NA223L), and the Oregon State University Edwards Endowment. Y.C. is partially supported by the China Scholarship Council.

REFERENCES

ABLOWITZ, M. J. & SEGUR, H. 1981 *Solitons and the Inverse Scattering Transform*. SIAM.

BYATT-SMITH, J. G. B. 1971 An integral equation for unsteady surface waves and a comment on the Boussinesq equation. *J. Fluid Mech.* **49**, 625–633.

CHAMBAREL, J., KHARIF, C. & TOUBOUL, J. 2009 Head-on collision of two solitary waves and residual falling jet formation. *Nonlinear Process. Geophys.* **16**, 111–122.

CHAN, R. K. C. & STREET, R. L. 1970 A computer study of finite-amplitude water waves. *J. Comput. Phys.* **6**, 68–94.

CHEN, Y., ZHANG, E. & YEH, H. 2014 Laboratory experiments on counter-propagating head-on collisions of solitary waves. Part 2: flow field. *J. Fluid Mech.* (submitted).

COOKER, M. J., WEIDMAN, P. D. & BALE, D. S. 1997 Reflection of a high amplitude solitary wave at a vertical wall. *J. Fluid Mech.* **342**, 141–158.

CRAIG, W., GUYENNE, P., HAMMACK, J., HENDERSON, D. & SULEM, C. 2006 Solitary water wave interactions. *Phys. Fluids* **18**, 057106.

DIORIO, J. D., LIU, X. & DUNCAN, J. H. 2009 An experimental investigation of incipient spilling breakers. *J. Fluid Mech.* **633**, 271–283.

DUNCAN, J. H., PHILOMIN, V., BEHRES, M. & KIMMEL, J. 1994 The formation of spilling breaking water waves. *Phys. Fluids* **6**, 2558–2560.

DUNCAN, J. H., QIAO, H., PHILOMIN, V. & WENZ, A. 1999 Gentle spilling breakers: crest profile evolution. *J. Fluid Mech.* **379**, 191–222.

FENTON, J. & RIENECKER, M. 1982 Fourier method for solving nonlinear water-wave problems: application to solitary-wave interactions. *J. Fluid Mech.* **118**, 411–443.

GORING, D. & RAICHLEN, F. 1980 The generation of long waves in the laboratory. In *Proceedings 17th International Conference on Coastal Engineering, Sydney, Australia* (ed. B. L. Edge), ASCE.

GRIMSHAW, R. 1971 The solitary wave in water of variable depth. Part 2. *J. Fluid Mech.* **46**, 611–622.

HAMMACK, J., HENDERSON, D., GUYENNE, P. & YI, M. 2004 Solitary-wave collisions. *Phys. Fluids* **18**, 057106.

LI, W. 2012 Amplification of solitary waves along a vertical wall. PhD thesis, Oregon State University.

LI, W., YEH, H. & KODAMA, Y. 2011 On the Mach reflection of a solitary wave: revisited. *J. Fluid Mech.* **672**, 326–357.

LIU, X. & DUNCAN, J. H. 2006 An experimental study of surfactant effects on spilling breakers. *J. Fluid Mech.* **567**, 433–455.

MAXWORTHY, T. 1976 Experiments on collisions between solitary waves. *J. Fluid Mech.* **76**, 177–185.

RAMSDEN, J. D. 1993 Tsunamis: forces on a vertical wall caused by long waves, bores, and surges on a dry bed. PhD thesis, California Institute of Technology.

RENOUARD, D., SANTOS, F. & TEMPERVILLE, A. 1985 Experimental study of the generation, damping, and reflexion of a solitary wave. *Dyn. Atmos. Oceans* **9**, 341–358.

SU, C. & MIRIE, R. M. 1980 On head-on collisions between two solitary waves. *J. Fluid Mech.* **98**, 509–525.

TANAKA, M. 1993 Mach reflection of a large-amplitude solitary wave. *J. Fluid Mech.* **248**, 637–661.

WEIDMAN, P. & MAXWORTHY, T. 1978 Experiments on strong interactions between solitary waves. *J. Fluid Mech.* **85**, 417–431.

YEH, H. & GHAZALI, A. 1986 A bore on a uniformly sloping beach. In *Proceedings 20th International Conference on Coastal Engineering* (ed. B. L. Edge), pp. 877–888. ASCE.

ZABUSKY, N. J. & KRUSKAL, M. D. 1965 Interaction of 'solitons' in a collisionless plasma and the recurrence of initial states. *Phys. Rev. Lett.* **15**, 240–243.